

# Computational Design and Preparation of Cation-Disordered Oxides for High-Energy-Density Li-Ion Batteries

Alexander Urban, Ian Matts, Aziz Abdellahi, and Gerbrand Ceder\*

Cation-disordered lithium-excess metal oxides have recently emerged as a promising new class of high-energy-density cathode materials for Li-ion batteries, but the exploration of disordered materials has been hampered by their vast and unexplored composition space. This study proposes a practical methodology for the identification of stable cation-disordered rocksalts. Here, it is established that the efficient method, which makes use of special quasirandom structures, correctly predicts cation-ordering strengths in agreement with accurate Monte-Carlo simulations and experimental observations. By applying the approach to the composition space of ternary oxides with formula unit  $\text{LiA}_{0.5}\text{B}_{0.5}\text{O}_2$  (A, B: transition metals), this study discovers a previously unknown cation-disordered structure,  $\text{LiCo}_{0.5}\text{Zr}_{0.5}\text{O}_2$ , that may function as the basis for a new class of cation-disordered cathode materials. This computational prediction is confirmed experimentally by solid-state synthesis and subsequent characterization by powder X-ray diffraction demonstrating the potential of the computational screening of large composition spaces for accelerating materials discovery.

## 1. Introduction

On the search for improved lithium-ion battery materials with greater energy density, cation-disordered lithium-excess transition-metal oxides have recently emerged as a promising new materials class for high-capacity cathodes.<sup>[1–9]</sup> In contrast to conventional well-ordered transition-metal-based cathode materials, such as layered  $\text{LiCoO}_2$ <sup>[10]</sup> or  $\text{LiMn}_2\text{O}_4$  spinels,<sup>[11]</sup> these new materials form in the disordered rocksalt structure such that lithium (Li) and transition-metal (TM) cations share the same sublattice. Percolation theory predicts<sup>[1,12]</sup> that a necessary prerequisite for Li transport in cation-disordered oxides is an excess of Li over TM of at least 10%, a concept which has

also been experimentally verified.<sup>[1,7]</sup> This is in line with the general strategy to utilize Li-excess chemistries to achieve higher energy densities.<sup>[13–15]</sup> However, Li-excess materials often suffer from structural instabilities that give rise to phase transitions and degradation upon repeated cycling.<sup>[16–19]</sup> As a possible remedy, cation disorder was found to enhance the structural stability upon Li extraction, which makes it possible to achieve high reversible capacities and reduces the overall volume change with varying lithium content.<sup>[1]</sup> Minimizing volume fluctuations is beneficial for all electrodes, but is especially important for solid-state batteries in order to prevent fracturing of the solid/solid electrode/electrolyte interfaces,<sup>[20,21]</sup> and as such cation-disordered electrodes are particularly attractive for all-solid batteries.

The stringent electronic structure requirements on TM ions in structures that need to remain well layered<sup>[22,23]</sup> have limited the active chemistry of cathode oxides to just a few elements such as Co and Ni. On the other hand, the composition space for potential cation-disordered oxides is vast, as TM mobility is not a constraint. Indeed, many of the new disordered cathodes contain elements such as Cr, Mo, Ti, and Nb, which were usually not used in well-ordered cathodes. Because of this, identifying the compositions of new cation-disordered oxides is a critical bottleneck for the discovery of improved disordered cathode materials. One successful strategy for the rational design of new cation-disordered Li-excess cathode materials has been to introduce excess Li into known stoichiometric disordered compositions, such as  $\text{LiTi}_{0.5}\text{Ni}_{0.5}\text{O}_2$ <sup>[8,24,25]</sup> and  $\text{LiTi}_{0.5}\text{Fe}_{0.5}\text{O}_2$ .<sup>[7,26,27]</sup> This approach is, however, limited by the small number of presently known cation-disordered Li-TM oxides. While it is in some cases possible to impose cation disorder to otherwise ordered crystal structures by means of mechanochemical synthesis routes,<sup>[28]</sup> a complete library of materials that potentially form in the disordered rocksalt structure would accelerate the development of cation-disordered cathode materials.

With this motivation in mind, the objective of the present work is to introduce a straightforward methodology for the computational prediction of new disordered rocksalts and to demonstrate its practicality by identifying and synthesizing a novel cation-disordered oxide. In the following Section 2 the computational methods, synthesis procedures, and characterization techniques are outlined. This is followed by a report of

Dr. A. Urban, Prof. G. Ceder  
Department of Materials Science and Engineering  
University of California  
Berkeley, CA 94720, USA  
E-mail: gceder@berkeley.edu

I. Matts, Dr. A. Abdellahi  
Department of Materials Science and Engineering  
Massachusetts Institute of Technology  
Cambridge, MA 02139, USA

Prof. G. Ceder  
Materials Science Division  
Lawrence Berkeley National Laboratory  
Berkeley, CA 94720, USA



DOI: 10.1002/aenm.201600488

the computational analyses in Section 3. After discussing the computational observations in Section 4, one of the predictions is experimentally verified in Section 5 by synthesis and characterization.

## 2. Methods

### 2.1. Density-Functional Theory Calculations

Electronic density-functional theory (DFT)<sup>[29,30]</sup> provides a reliable standard for the evaluation of structural energies. All reported DFT calculations are based on the gradient corrected functional by Perdew et al.<sup>[31,32]</sup> within the projector-augmented wave approach<sup>[33]</sup> as implemented in the Vienna Ab-Initio Simulation Package.<sup>[34,35]</sup> The rotationally averaged Hubbard U correction<sup>[36,37]</sup> (DFT+U) was used to correct the self-interaction error in oxides containing the species Ag, Co, Cr, Cu, Fe, Mn, Mo, Nb, Ni, and V. The values of the U parameters, which are essentially taken from reference,<sup>[38]</sup> are given in Table S1 in the Supporting Information. DFT energies and atomic forces were generally converged to 0.05 meV per atom and 50 meV Å<sup>-1</sup>. Gamma-centered k-point meshes with a density of 1000 divided by the number of atoms were used for Brillouin-zone integration, and the cutoff for the plane-wave expansion of the wave functions was 520 eV.<sup>[39]</sup>

### 2.2. Monte-Carlo Simulations

The rocksalt structure is the combination of two face-centered cubic (FCC) sublattices, which are in the case of lithium metal oxides occupied by oxygen and the cations (Li, TM), respectively. Since the oxygen sublattice is independent of the cation ordering, the configurational space of rocksalt-type oxides can be reduced to the cation (FCC) sublattice.<sup>[12]</sup>

To enable a thorough sampling of cation distributions, we mapped the configurational energy onto a cluster-expansion (CE) lattice model<sup>[40–42]</sup> as implemented in the Clusters Approach to Statistical Mechanics (CASM) software.<sup>[43–46]</sup> In the CE approach, the configurational energy is expanded in effective cluster interactions (ECIs),  $J_\alpha$ , that correspond to different combinations (clusters) of sites  $C_\alpha$ . The configurational energy  $E$  can then be expressed as

$$E = E_0 + \sum_{\alpha} J_{\alpha} \Pi_{\alpha} \quad \text{with} \quad \Pi_{\alpha} = \frac{1}{N} \sum_{C_{\alpha} \in \alpha} \prod_{\sigma_i \in C_{\alpha}} \sigma_i, \quad (1)$$

where  $E_0$  is a constant energy term, the products over site occupancies  $\Pi_{\alpha}$  for each class of clusters  $\alpha$  are the cluster correlations, and  $N$  is the size of the supercell in terms of multiples of the primitive FCC unit cell.

We followed the convention of the Ising model, representing the site occupation by a symmetric pseudo spin variable so that  $\sigma_i \in \{-1, +1\}$  for the binary oxides (LiAO<sub>2</sub>) and  $\sigma_i \in \{-1, 0, +1\}$  for the ternary oxides (LiA<sub>0.5</sub>B<sub>0.5</sub>O<sub>2</sub>). With this convention, all cluster correlations are exactly equal to zero for a random cation distribution in the binary LiAO<sub>2</sub> oxides, and hence the energy of the random state is given by  $E_{\text{random}} = E_0$ . There is

no such simple relationship for the ternary LiA<sub>0.5</sub>B<sub>0.5</sub>O<sub>2</sub> oxides, so that the energy of the random state was obtained by direct evaluation of size-converged random configurations.

Each CE Hamiltonian was fitted to the DFT energies of the optimized geometries of about 100 configurations generated by a systematic structure enumeration.<sup>[47–49]</sup> The resulting cross-validation scores of the lattice models are between 9 and 24 meV per cation (see Table S2 and Figure S1 in the Supporting Information). The compressive sensing paradigm was used to fit the system-specific ECIs.<sup>[50]</sup>

### 2.3. Special Quasirandom Structures

Special quasirandom structures (SQSs) are structures with small periodic unit whose atomic distributions are chosen such that the cluster correlations  $\Pi_{\alpha}$  of Equation (1) approach the expected value in a random atomic arrangement as closely as possible for a given structure size.<sup>[51]</sup> In the alloy community, SQSs have been, for example, successfully used to evaluate mixing enthalpies<sup>[52]</sup> and to model the electronic structure of random alloys.<sup>[53]</sup>

To model the random state of the LiAO<sub>2</sub> composition, we use an SQS originally constructed for the investigation of solid solution energies in disordered FCC alloys.<sup>[54]</sup> This SQS is appropriate for the description of the FCC cation sublattice in rocksalt-type oxides when oxygen sites are added. Although the SQS only contains 16 cation sites, it reproduces the energies of the random state, as obtained from CE Hamiltonians, with a remarkable accuracy that is of the same order of magnitude as the cross-validation scores of the CE fits (see Figure S3 in the Supporting Information). For the LiA<sub>0.5</sub>B<sub>0.5</sub>O<sub>2</sub> composition, we employed an SQS with 32 cation sites that was originally constructed by Shin et al. for the investigation of ternary FCC alloy solution phases<sup>[52]</sup> and also provides excellent estimates of the random state energy (Figure S3, Supporting Information).

Note that SQSs for other compositions can be efficiently constructed by optimizing the cluster correlations for a given structure size, for example using simulated annealing.<sup>[55]</sup>

## 3. Results

While our objective is to develop a computationally efficient approach for the prediction of cation disorder, we first seek to establish accurate estimates of the cation-ordering strengths before motivating an approximate methodology. In the following Section 3.1, we therefore introduce the temperature of the configurational order–disorder (OD) phase transition, which can be obtained through direct Monte-Carlo (MC) simulations, as a measure of the intrinsic cation-ordering strength. In Section 3.2, we subsequently propose a computationally less demanding scheme that can provide equivalent information.

### 3.1. Estimating the Cation-Ordering Strength Based on the Configurational Order–Disorder Transition

Whether a lithium metal oxide forms in an ordered, cation-segregated structure or in the cation-disordered rocksalt structure is determined by the thermodynamically most stable phase at

synthesis conditions (e.g., depending on the synthesis temperature). In the case of a weakly ordered material, the synthesis temperature may exceed the temperature of the OD transition, so that the disordered phase is entropy-stabilized over the ordered low-temperature ground state during the synthesis. Hence, the OD transition temperature can be understood as a measure of the intrinsic cation-ordering strength in a material.

In experiments, the OD transition in Li-TM oxides can only be observed if it occurs below the melting or decomposition temperatures. As a consequence, the cation-ordering strength can experimentally only be obtained for weakly ordered materials. In computer simulations, on the other hand, it is possible to prevent the material from undergoing melting or decomposition so that estimates of the OD transition temperature may be obtained even where this phase transition is experimentally inaccessible. Note, however, that such effective temperatures of hypothetical OD transitions do not have any counterpart in real life and may only serve as a proxy for the cation-ordering strength. As such, reported values for OD transition temperatures are nonphysical in most cases, and thus not possible to observe or reproduce experimentally.

Using the CE lattice models described in Section 2.2, we carried out direct MC simulations of the OD phase transitions in the stoichiometric lithium oxides of first-row transition metals. Note that the lattice models do not account for vibrational and electronic degrees of freedom, so that these contributions to the entropy are not included in our simulations. While this approximation may give rise to an error in the absolute OD transition temperatures, the relative ranking of the cation-ordering strengths can be expected to be dominated by the configurational contributions to the entropy, so the ordinal ranking will not be influenced.

All MC simulations were initialized in the ordered  $\text{LiAO}_2$  ( $A$  = transition metal) ground state which was then heated from 100 K until above the OD phase transition followed by cooling to 100 K to record potential hysteresis. The cation-ordered

structure of most Li-TM oxides is either the layered  $\alpha$ - $\text{NaFeO}_2$  structure shown in Figure 1a ( $\text{LiVO}_2$ ,  $\text{LiCrO}_2$ ,  $\text{LiCoO}_2$ ,  $\text{LiNiO}_2$ ,  $\text{LiCuO}_2$ ) or the  $\gamma$ - $\text{LiFeO}_2$  structure shown in Figure 1b ( $\text{LiScO}_2$ ,  $\text{LiFeO}_2$ ).<sup>[56]</sup> The ordered ground state of  $\text{LiMnO}_2$  is orthorhombic,<sup>[56]</sup> and no cation-ordered phase is known for  $\text{LiTiO}_2$  as prepared via solid-state synthesis routes. All known ordered ground state phases are correctly reproduced by our computational structure enumeration and by the CE models. In addition, DFT calculations predict the  $\gamma$ - $\text{LiFeO}_2$  structure to be the most stable  $\text{LiTiO}_2$  phase at 0 K.

To illustrate the MC procedure, the internal energy and specific heat during MC simulations of  $\text{LiCrO}_2$  and  $\text{LiNiO}_2$  are shown in Figure 2. An equivalent visualization of the energies during the MC simulations of the other oxides can be found in Figure S2 in the Supporting Information. As indicated in Figure 2, the OD phase transition gives rise to an inflection point (second-order transition) or discontinuity (first order transition) in the internal energy and a peak in the specific heat.

The zero-point of the energy axis of Figure 2a corresponds to the energy of a random cation distribution, which is, as discussed in Section 2.2, given by the constant  $E_0$  term of the CE models. As seen in the figure, the energy of the cation-disordered phase is significantly lower than the energy of the random state. This stabilization can be attributed to system-specific short-range ordering that is still present in the cation-disordered phase.

The obtained cation-ordering strengths for  $\text{LiAO}_2$  with  $A = \text{Sc, Ti, V, Cr, Mn, Fe, Co, Ni, and Cu}$  in terms of effective DO transition temperatures  $T_c$  are listed in Table 1.

### 3.2. Rapid Disordering Estimates Based on Special Quasirandom Structures

The direct MC simulation approach of the previous section is useful as an accurate baseline for the prediction of the cation-ordering strength, but the methodology is too involved

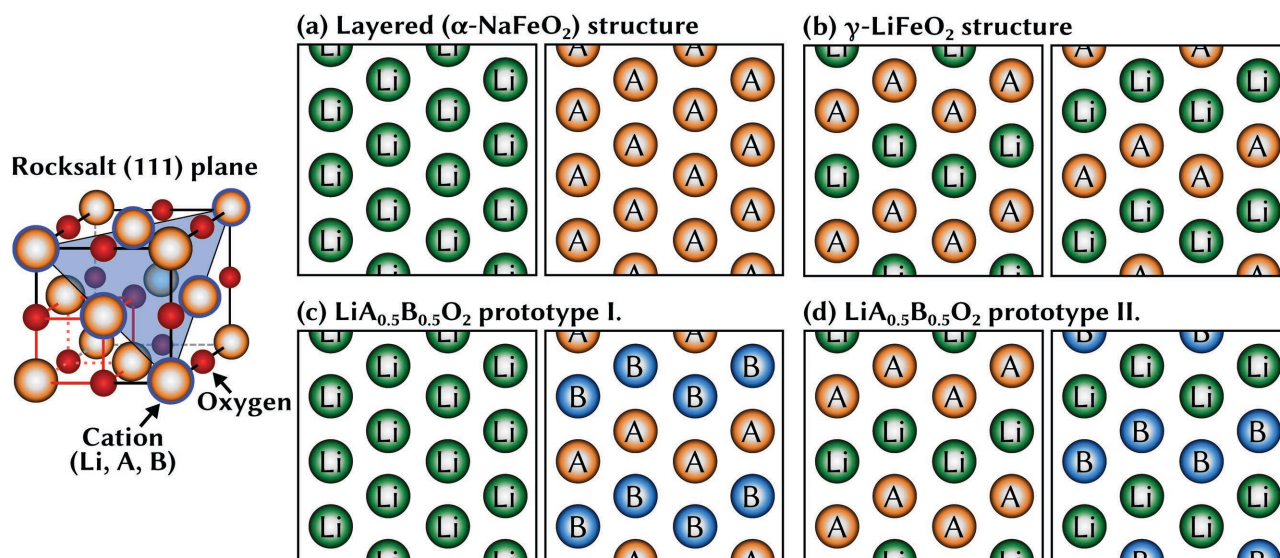


**Figure 1.** Atomic orderings in cation layers of the two most common  $\text{LiAO}_2$  ground state configurations: a) the layered ( $\alpha$ - $\text{NaFeO}_2$ ) structure and b) the  $\gamma$ - $\text{LiFeO}_2$  structure. Panels c) and d) show the two related prototypes for the  $\text{LiA}_{0.5}\text{B}_{0.5}\text{O}_2$  compositions. A cation layer within the rocksalt structure is highlighted in the structure model on the left.

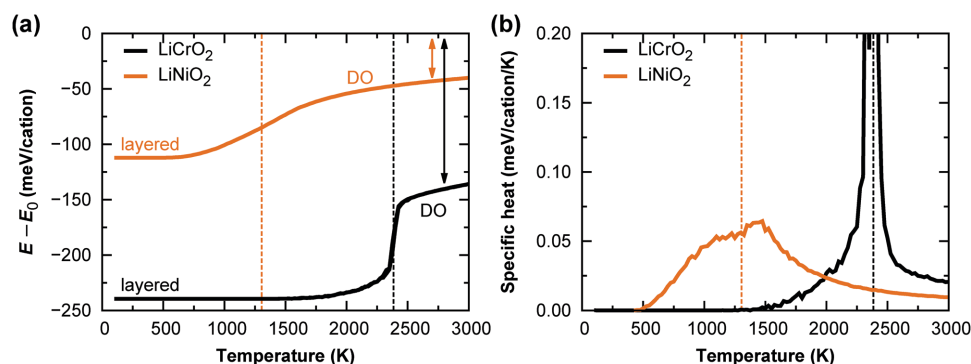


**Figure 2.** a) Energy and b) specific heat during Monte-Carlo simulations using cluster-expansion models of  $\text{LiCrO}_2$  (solid orange line) and  $\text{LiNiO}_2$  (dashed blue line). The phase transitions from the order ground states (layered) to the cation-disordered state (DO) are indicated by vertical dashed lines. The amount of stabilization due to short-range ordering is shown as arrows. The energy of a random cation distribution ( $E_0$ ) is the zero-point for the energy.

for the systematic screening of larger composition spaces. The construction of higher-order lattice models for Li-TM oxides with two or more different TM species is time consuming and computationally demanding. Hence, a more approximate approach for estimating the cation-ordering strength is required for practical purposes.

An intuitive quantity that is related to the stability of the ordered ground state of a material is the energy difference between the disordered state and the ordered state. Based on our insight from the Li-TM oxides of the previous section, the energy of the ordered ground state of any  $\text{LiAO}_2$  is either the layered  $\alpha\text{-NaFeO}_2$  structure, the  $\gamma\text{-LiFeO}_2$  structure, or the orthorhombic  $\text{LiMnO}_2$  structure. Hence, the evaluation of the ground state energy requires only three DFT calculations of structures with small periodic units. However, there is no obvious way to estimate the energy of the cation-disordered phase including its stabilization due to short-range ordering without the MC sampling of the previous section.

The energy of a random cation distribution can, on the other hand, be estimated with good accuracy using SQSs as described

**Table 1.** Cation-ordering strengths for different lithium transition-metal oxides in effective temperature units as obtained from Monte-Carlo heating and cooling simulations. The initial ordered ground state phases are given in terms of their prototypes. Free-energy integration was performed to remove the hysteresis between heating and cooling for  $\text{LiScO}_2$ ,  $\text{LiMnO}_2$ ,  $\text{LiFeO}_2$ , and  $\text{LiCuO}_2$ .

	Ordered Phase	$T_c$ [K]
$\text{LiScO}_2$	$\gamma\text{-LiFeO}_2^{\text{a)}$	1665 <sup>c)</sup>
$\text{LiTiO}_2$	$\gamma\text{-LiFeO}_2^{\text{b)}$	805
$\text{LiVO}_2$	$\alpha\text{-NaFeO}_2^{\text{a)}$	1775
$\text{LiCrO}_2$	$\alpha\text{-NaFeO}_2^{\text{a)}$	2385
$\text{LiMnO}_2$	Orthorhombic <sup>a)</sup>	1370 <sup>c)</sup>
$\text{LiFeO}_2$	$\gamma\text{-LiFeO}_2^{\text{a)}$	2265 <sup>c)</sup>
$\text{LiCoO}_2$	$\alpha\text{-NaFeO}_2^{\text{a)}$	6415
$\text{LiNiO}_2$	$\alpha\text{-NaFeO}_2^{\text{a)}$	1305
$\text{LiCuO}_2$	$\alpha\text{-NaFeO}_2^{\text{a)}$	2770 <sup>c)</sup>

<sup>a)</sup>From ref. [56]; <sup>b)</sup>From this work; <sup>c)</sup>From free-energy integration.

in Section 2.3. The SQS from reference [54] reproduces the energy of the random  $\text{LiAO}_2$  state with an accuracy that is comparable to the error in the CE models of the previous section (see Figure S3 in the Supporting Information).

As seen in **Figure 3**, the energy difference between the SQS and the ordered ground state correlates linearly with the critical temperature of the OD transition for the  $\text{LiAO}_2$  of the previous section. The remaining uncertainty in the ranking of the ordering strength is of the same order of magnitude as the errors in the CE lattice models, and as such the predictive power of the SQS estimate is comparable to the results of the MC simulations while being computationally far less demanding.

### 3.3. Screening of the $\text{LiA}_{0.5}\text{B}_{0.5}\text{O}_2$ Composition Space

Having arrived at a computationally efficient methodology to predict the cation-ordering strength in Li-TM oxides, we proceed to apply the method to the ternary composition space of mixed  $\text{LiAO}_2\text{-LiBO}_2$  oxides ( $A, B =$  first and second row TMs) to identify those  $\text{LiA}_{0.5}\text{B}_{0.5}\text{O}_2$  that are most likely to form as

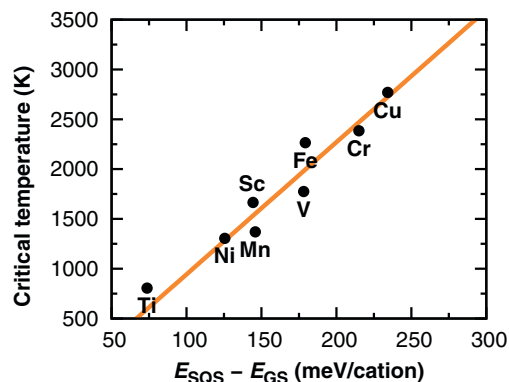


**Figure 3.** Correlation of the energy difference between the ordered ground state and the cation disordered phase as modeled by SQS with the temperature of the order-disorder phase transition in different lithium transition-metal oxides. The orange trend line is a linear fit to the data points.  $\text{LiCoO}_2$  is omitted for clarity, as its phase transition occurs above 6000 K.

disordered rocksalts. For this screening, we employed the SQS of reference [52] as discussed in Section 2.3.

To estimate the energy of the ordered  $\text{LiA}_{0.5}\text{B}_{0.5}\text{O}_2$  ground state, we determined the lowest-energy cation orderings of  $\text{LiMn}_{0.5}\text{Ni}_{0.5}\text{O}_2$ , a prototypical ternary layered oxide, and  $\text{LiNi}_{0.5}\text{Ti}_{0.5}\text{O}_2$  which forms as disordered rocksalt, by structure enumeration up to cell sizes with 8 cations. The ground-state orderings determined in this fashion are shown in Figure 1c,d. The most stable  $\text{LiMn}_{0.5}\text{Ni}_{0.5}\text{O}_2$  configuration (Figure 1c) can be derived from the layered  $\alpha\text{-NaFeO}_2$  structure by substituting Mn for half of the Ni in  $\text{LiNiO}_2$ . Similarly, the most stable  $\text{LiNi}_{0.5}\text{Ti}_{0.5}\text{O}_2$  ordering (Figure 1d) is related to the  $\gamma\text{-LiFeO}_2$  structure and can be constructed by replacing half of the Ti in  $\text{LiTiO}_2$  with Ni. Note that, in the case of  $\text{LiMn}_{0.5}\text{Ni}_{0.5}\text{O}_2$ , a more complex  $2\sqrt{3}a \times 2\sqrt{3}a$  ordering with a periodicity that exceeds the cell size considered in the present work was previously found to be slightly lower in energy (by 0.5 meV per formula unit) than the zig-zag ordering of Figure 1c.<sup>[57]</sup> Hence, we cannot guarantee that the ordered ground state of every  $\text{LiA}_{0.5}\text{B}_{0.5}\text{O}_2$  is among these two configurations. It can be expected, however, that based on the analogy with the binary  $\text{LiAO}_2$  ground states the ternary ground state energy is close to the energy of the more stable one of these two prototypes.

The predicted cation-ordering strengths for 136 different  $\text{LiA}_{0.5}\text{B}_{0.5}\text{O}_2$  based on the energy difference between the SQS and the ground state estimate are visualized in Figure 4. In the figure, every TM combination is represented by a circle, and the radius of the circle indicates the cation-disordering strength such that the radius is smallest for the material with the strongest cation ordering and largest for the material that is most likely to be cation disordered. In addition to the cation-ordering strength, the color of each circle in Figure 4 encodes the mixing enthalpy with respect to oxides with TM oxidation states between 2 and 4

$$E_{\text{mix}}(\text{LiA}_{0.5}\text{B}_{0.5}\text{O}_2) = \max(E_{\text{mix}}^{(1)}, E_{\text{mix}}^{(2)}, E_{\text{mix}}^{(3)}) \quad \text{with} \quad (2)$$

$$E_{\text{mix}}^{(1)} = E_{\text{GS}}(\text{LiA}_{0.5}\text{B}_{0.5}\text{O}_2) - 0.5E_{\text{GS}}(\text{LiAO}_2) - 0.5E_{\text{GS}}(\text{LiBO}_2)$$

$$E_{\text{mix}}^{(2)} = E_{\text{GS}}(\text{LiA}_{0.5}\text{B}_{0.5}\text{O}_2) - 0.5E_{\text{GS}}(\text{AO}) - 0.5E_{\text{GS}}(\text{Li}_2\text{BO}_3)$$

$$E_{\text{mix}}^{(3)} = E_{\text{GS}}(\text{LiA}_{0.5}\text{B}_{0.5}\text{O}_2) - 0.5E_{\text{GS}}(\text{Li}_2\text{AO}_3) - 0.5E_{\text{GS}}(\text{BO})$$

as a proxy for the stability of the ternary oxide. Generally, the formation energy of ternary oxides can be reliably predicted from binary oxides within DFT+U.<sup>[58]</sup> For those  $\text{LiA}_{0.5}\text{B}_{0.5}\text{O}_2$  that are predicted to decompose, the cation-ordering strength is evaluated with respect to the decomposition products, i.e., the energy difference between the SQS and the energy of the decomposition products is considered. Note that the free energy

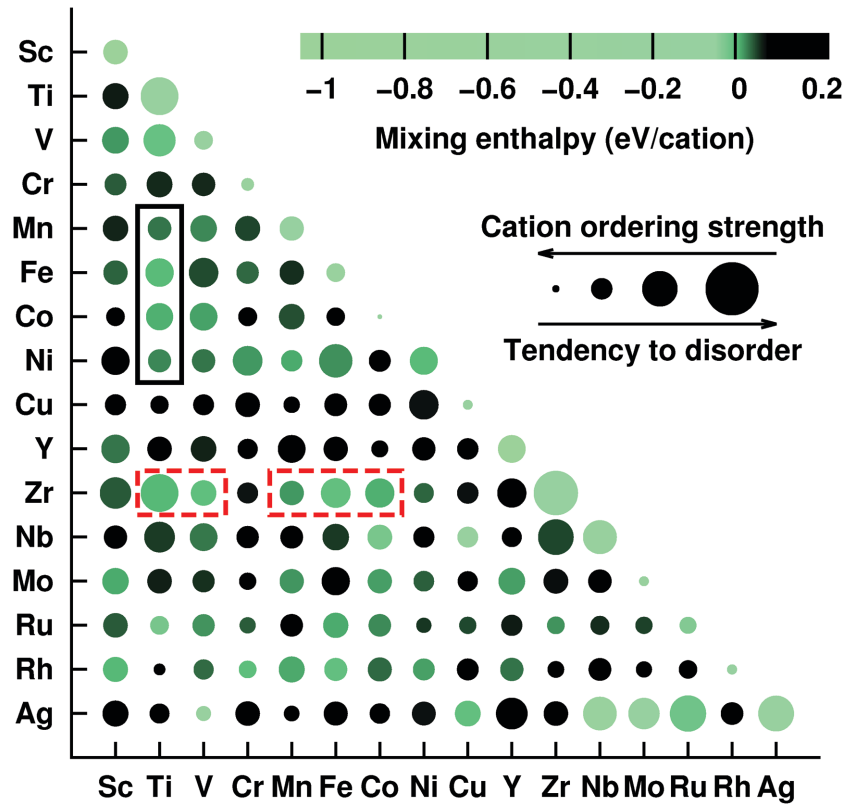


**Figure 4.** Screening results for the  $\text{LiA}_{0.5}\text{B}_{0.5}\text{O}_2$  composition space. Each combination  $AB$  of transition metals is represented by a circle. The color of the circle visualizes the predicted stability in terms of the estimated mixing enthalpy (bright green: more stable; dark: less stable), and the size of the circle indicates the tendency to disorder (small circle: strongly ordered; large circle: likely disordered).

of an ideal solid solution of the two end member phases is stabilized by the mixing entropy on the cation sublattice

$$S_{\text{mix}} = -k_B(x_A \ln x_A + x_B \ln x_B) = k_B \ln 2, \quad (3)$$

where  $x_A$  and  $x_B$  are the concentrations of species A and B (both 0.5), and  $k_B$  is Boltzmann's constant. We consider all materials with a positive mixing enthalpy greater than  $1000^\circ\text{C} \cdot S_{\text{mix}} \approx 75$  meV per cation to be thermodynamically inaccessible during solid state synthesis, and those TM combinations are colored black in Figure 4.

#### 4. Discussion of the Computational Results

In the previous sections, we conceived a rapid computational methodology for the identification of cation-disordered Li-TM oxide compositions and demonstrated that the relative cation-ordering strength predicted by the approach agrees well with direct MC simulations of the OD transition. Apart from this computational consistency, the predicted trends in the ordering strength of binary Li-TM oxides ( $\text{LiAO}_2$ ) are also in agreement with experimental observations: Layered  $\text{LiCoO}_2$ , the material with the greatest predicted cation-ordering strength, is known to be highly stable,<sup>[28,59]</sup> whereas  $\text{LiTiO}_2$  forms in the disordered

rocksalt phase in solid-state synthesis,<sup>[56]</sup> in agreement with the predicted weak cation ordering. In the case of layered LiNiO<sub>2</sub>, which has the second lowest predicted ordering strength, cation mixing between the Li and Ni layers is a well-known phenomenon<sup>[60]</sup> and mechanochemical cation disordering has been reported to be facile.<sup>[28]</sup>

Further confirmation for the computational cation-ordering strength comes from the results for the ternary LiA<sub>0.5</sub>B<sub>0.5</sub>O<sub>2</sub> oxides: The computational screening reliably identified the cation-disordered materials based on Ti oxides (general formula LiTi<sub>x</sub>B<sub>1-x</sub>O<sub>2</sub>; highlighted with a black rectangle in Figure 4).<sup>[7,8,24–27,61]</sup> Note that the known disordered Nb oxides<sup>[5,6,62]</sup> are based on Li<sub>3</sub>NbO<sub>4</sub> (i.e., Nb<sup>5+</sup>) and are therefore not included in our screening, as the LiNb<sub>0.5</sub>B<sub>0.5</sub>O<sub>2</sub> calculations converged to Nb<sup>4+</sup> (with the exception of LiNb<sub>0.5</sub>Ag<sub>0.5</sub>O<sub>2</sub>).

One apparent discrepancy between the computational predictions and experiment is the cation-ordering strength in LiFeO<sub>2</sub>. While the  $\gamma$ -LiFeO<sub>2</sub> structure is the most stable ordered LiFeO<sub>2</sub> phase, LiFeO<sub>2</sub> has been reported to form as disordered rocksalt in solid state synthesis.<sup>[56,63]</sup> Based on this observation, one would expect the cation-ordering strength in LiFeO<sub>2</sub> to be smaller than predicted by our computations. However, the temperature for reduction of Fe(III) oxide to Fe(II) oxide is low in comparison to the oxides of the other transition metals,<sup>[64]</sup> so that it is likely that some Fe(II) oxide is formed at synthesis conditions. Such side reactions and the resulting increase in configurational entropy are not captured by our simulations and may explain the observed disagreement.

We also note that Zr does not occur in oxidation state 3, so that LiZrO<sub>2</sub> is merely a hypothetical composition.

In addition to reproducing known materials, the results from the previous section also predict entirely new disordered rocksalts. As seen in Figure 4, among the materials predicted to exhibit the weakest cation ordering are several Rh and Ag containing oxides, such as LiAg<sub>0.5</sub>Ti<sub>0.5</sub>O<sub>2</sub> and LiRh<sub>0.5</sub>Zr<sub>0.5</sub>O<sub>2</sub>. Owing to the low earth abundance of these two transition metals and to their lack of utilizable redox activity, these materials are of low interest for battery applications. However, the screening results also identify several other weakly ordered materials based on Zr oxides that are more attractive as cathode materials (highlighted with red dashed rectangles in Figure 4). In particular, LiZr<sub>0.5</sub>B<sub>0.5</sub>O<sub>2</sub> with B = Mn, Fe, and Co are appealing because of the accessible TM redox couples. We will investigate one of the Zr-based oxides, LiZr<sub>0.5</sub>Co<sub>0.5</sub>O<sub>2</sub>, in more detail in the following section 5.

A common assumption during synthesis planning is that atomic species with very different ionic radii are likely to segregate, whereas mixing on a common sublattice can be expected for ions with similar radii. Based on the LiA<sub>0.5</sub>B<sub>0.5</sub>O<sub>2</sub> data from the previous section, we can now assess the reliability of this simple heuristic. Note that the ionic radius depends on the oxidation state, and in principle the TM valence has to be guessed based on chemical intuition if no electronic structure calculation is performed. Here, we can deduce the valence state of each TM ion from its atomic magnetization, i.e., the integrated spin density around individual atoms. Indeed, in the case of the Zr oxides, the Shannon radii of the transition metal ions are similar to each other (Zr<sup>4+</sup>: 72 pm, Cr<sup>2+</sup>: 73 pm, Co<sup>2+</sup>: 75 pm) and to the ionic radius of Li<sup>+</sup> (76 pm).<sup>[65]</sup> However, this simple

relationship is not always obeyed. For example, LiTi<sub>0.5</sub>Zr<sub>0.5</sub>O<sub>2</sub> is predicted to be likely disordered, but Ti<sup>2+</sup> and Zr<sup>4+</sup> are with 86 and 72 pm significantly different. In LiNb<sub>0.5</sub>Ag<sub>0.5</sub>O<sub>2</sub>, which is predicted to be among the least strongly ordered materials, the ionic radii of the transition metals (115 pm for Ag<sup>1+</sup> and 64 pm for Nb<sup>5+</sup>) are also very different. These examples show that the ionic radius heuristic alone is not generally sufficient to predict cation disorder and the stability of mixed phases.

We note, though, that the stability of compositions containing TMs that favor oxidation states other than 2, 3, and 4 may be overestimated in Figure 4, as only these oxidation states are considered by the mixing enthalpy as defined in Equation (2).

Finally, we note that the present methodology does not cover oxides that only disorder upon lithium extraction, such as Li-excess Mo-Cr oxide.<sup>[1]</sup> However, such materials could be discovered by extending the screening to delithiated (A<sub>0.5</sub>B<sub>0.5</sub>O<sub>2</sub>) compositions.

## 5. Experimental Verification: Cation-Disordered LiCo<sub>0.5</sub>Zr<sub>0.5</sub>O<sub>2</sub>

To further confirm the computational methodology, we selected one promising composition for a deeper investigation. Out of the Zr-based materials (red dashed frames in Figure 4), the cation-ordering strength is predicted to be smallest in LiZr<sub>0.5</sub>B<sub>0.5</sub>O<sub>2</sub> with B = Ti, Fe, and Co. LiZr<sub>0.5</sub>Co<sub>0.5</sub>O<sub>2</sub> is particularly attractive for battery applications because of the Co<sup>2+/4+</sup> double redox that would in principle enable TM-redox limited capacities of up to 1 Li per formula unit. Using the Materials Project database<sup>[39,66–68]</sup> we determined that LiZr<sub>0.5</sub>Co<sub>0.5</sub>O<sub>2</sub> is unstable by 32 meV per cation with respect to decomposition into CoO and Li<sub>2</sub>ZrO<sub>3</sub> (in agreement with the mixing enthalpy of Equation (2)), which is well below the expected stabilization due to the mixing entropy, Equation (3), at synthesis temperatures. As a final computational check, we carried out MC simulations based on a full ternary cluster expansion Hamiltonian for LiCo<sub>0.5</sub>Zr<sub>0.5</sub>O<sub>2</sub>, an undertaking that is time consuming and computationally demanding so that it would not be feasible for a large number of compositions. The simulations confirm that the OD transition occurs at a similar temperature as in LiNi<sub>0.5</sub>Ti<sub>0.5</sub>O<sub>2</sub>, which is cation disordered as synthesized, and at far lower temperature than in the well-ordered LiNi<sub>0.5</sub>Mn<sub>0.5</sub>O<sub>2</sub> (see Figure S4 in the Supporting Information).

Having established confidence in our computational prediction, we attempted the actual preparation of the material. Using the solid-state synthesis method described in section 7, LiCo<sub>0.5</sub>Zr<sub>0.5</sub>O<sub>2</sub> with the rocksalt crystal structure was synthesized to 94.2% purity according to Rietveld refinement. The X-ray diffraction (XRD) spectrum for the as-synthesized sample is shown in Figure 5. The structure of rocksalt LiCo<sub>0.5</sub>Zr<sub>0.5</sub>O<sub>2</sub> is analogous to CoO (ICSD pattern 04-018-4843)<sup>[69,70]</sup> and was refined to the rocksalt structure. The CoO ICSD pattern was modified in Bruker TOPAS to reflect the composition of LiCo<sub>0.5</sub>Zr<sub>0.5</sub>O<sub>2</sub> (with the lattice parameters remaining the same) and a modified XRD spectrum was simulated and shown in Figure 5 (thick orange line). The main impurity phase present is Li<sub>2</sub>ZrO<sub>3</sub> (ICSD pattern 00-041-0324),<sup>[69,70]</sup> which is one of the calculated equilibrium phases at this composition (see the

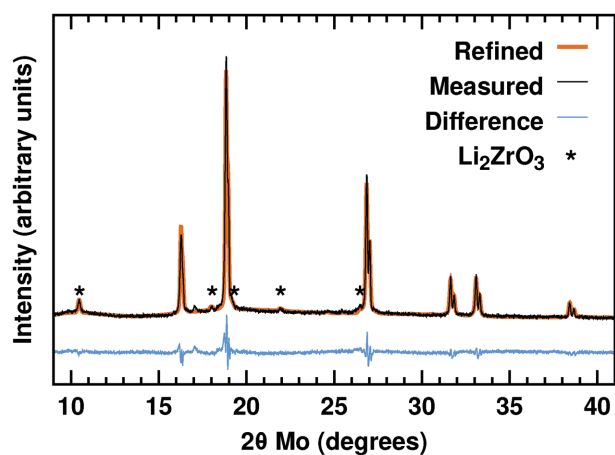


**Figure 5.** Unprocessed X-ray diffraction spectrum of as-synthesized  $\text{LiCo}_{0.5}\text{Zr}_{0.5}\text{O}_2$  (thin black line) and refined spectrum based on the disordered rocksalt structure and the  $\text{Li}_2\text{ZrO}_3$  impurity phase (thick orange line).  $\text{Li}_2\text{ZrO}_3$  peaks are indicated with stars. The double-peak intensities are due to signals from  $\text{Mo } K_{\alpha 1}$  and  $K_{\alpha 2}$  radiation.

computed phase diagram in Figure S5, Supporting Information). If it is assumed that no significant amount of Li, Co, or Zr, beyond the 7% Li molar excess, evaporated during synthesis and that all phases in the sample are crystalline, an approximate composition of the rocksalt phase may be extracted. If these assumptions are taken to be true and the phase fraction of  $\text{Li}_2\text{ZrO}_3$  is taken to be 5.8%, the amount determined by Rietveld refinement, the composition of the cation-disordered rocksalt phase is approximately  $\text{Li}_{0.97}\text{Co}_{0.55}\text{Zr}_{0.48}\text{O}_2$ . The composition as determined by mass spectrometry can be found in Table S3 in the Supporting Information.

## 6. Conclusions and Outlook

Here, we proposed a rapid approach utilizing special quasirandom structures for the computational identification of novel cation-disordered oxides. We assessed the predictive power of the method by comparison to direct MC simulations of the configurational OD transition before screening the composition space of ternary  $\text{LiA}_{0.5}\text{B}_{0.5}\text{O}_2$  for previously unknown disordered rocksalts. The results of this search (visualized in Figure 4) correctly identify known disordered rocksalts and predict an entirely new class of cation-disordered Zr-based compositions with the general composition  $\text{LiZr}_{0.5}\text{B}_{0.5}\text{O}_2$  ( $B = \text{Ti, V, Mn, Fe, Co}$ ). To verify this prediction and as a proof-of-concept, we prepared  $\text{LiCo}_{0.5}\text{Zr}_{0.5}\text{O}_2$  by solid state synthesis, confirming that it forms in the rocksalt structure.

This demonstrates the viability of a computational pre-screening of large composition spaces to accelerate the discovery of disordered rocksalts for Li-ion battery cathodes, and the approach developed in this article will likely enable the identification of further cation-disordered oxides by enlarging the chemical search space and by considering additional compositions.

By introducing lithium excess into cation-disordered  $\text{LiCo}_{0.5}\text{Zr}_{0.5}\text{O}_2$ , the material has the potential to function as

the basis for high-capacity Li-ion battery cathode materials with good structural integrity. Off-stoichiometric compositions based on stoichiometric cation-disordered materials typically also disorder, as has previously been demonstrated for the Li-Ni-Ti-O and Li-Ti-Fe-O chemistries.<sup>[7,8]</sup> In addition,  $\text{ZrO}_2$  is an efficient coating material for cathode particles,<sup>[71]</sup> which might hint at the possibility that  $\text{Zr}^{4+}$  oxides form protective surface layers upon oxygen loss, a common deterioration phenomenon observed in lithium-excess materials.<sup>[16–19]</sup> The exploration of lithium-excess chemistries and their electrochemical properties will therefore be the subject of future work.

## 7. Experimental Section

**Solid-State Synthesis:**  $\text{LiCo}_{0.5}\text{Zr}_{0.5}\text{O}_2$  was synthesized using a standard solid-state synthesis method. Stoichiometric amounts of  $\text{Li}_2\text{CO}_3$  (7% excess, Alfa Aesar, 99.0% min),  $\text{CoCO}_3$  (Alfa Aesar, 99.5%), and  $\text{Zr}(\text{OH})_4$  (Sigma-Aldrich, 97%) were thoroughly mixed in a Retsch PM200 planetary ball mill at 300 rpm for 4 h. The ball-milled precursor mixture was then heated to 900 °C under flow of Argon for 10 h and furnace cooled.

**Sample Characterization:** Phases present in the synthesized samples were identified by powder X-ray diffraction (XRD). XRD measurements were taken using a Bruker D8 Advance diffractometer (molybdenum  $K_{\alpha}$ ,  $\lambda = 0.7093 \text{ \AA}$ ), Bruker AXS, Germany) flipstick sample changer, scanning from 8° to 40°  $2\theta$ . Phase identification and spectrum refinement were completed using HighScore Plus software (PANalytical, The Netherlands). XRD spectra simulation and Rietveld refinement were done using Bruker TOPAS software (Bruker AXS, Germany).

## Supporting Information

Supporting Information is available from the Wiley Online Library or from the author.

## Acknowledgements

This work was supported by the Robert Bosch Corporation and by Umicore Specialty Oxides and Chemicals. The authors thank Stephen Dacek, Dong-Hwa Seo, Jinyuk Lee, Nongnuch Artrith, and Shou-Hang Bo for valuable discussions. This work used the Extreme Science and Engineering Discovery Environment (XSEDE), which is supported by National Science Foundation grant number ACI-1053575. In addition, resources of the National Energy Research Scientific Computing Center, a DOE Office of Science User Facility supported by the Office of Science of the U.S. Department of Energy under Contract No. DE-AC02-05CH11231, are gratefully acknowledged.

Received: March 2, 2016

Revised: April 9, 2016

Published online:

- [1] J. Lee, A. Urban, X. Li, D. Su, G. Hautier, G. Ceder, *Science* **2014**, 343, 519.
- [2] R. Chen, S. Ren, M. Knapp, D. Wang, R. Witter, M. Fichtner, H. Hahn, *Adv. Energy Mater.* **2015**, 5, 1401814.
- [3] S. Ren, R. Chen, E. Maawad, O. Dolotko, A. A. Guda, V. Shapovalov, D. Wang, H. Hahn, M. Fichtner, *Adv. Sci.* **2015**, 2, 1500128.
- [4] R. Chen, S. Ren, M. Yavuz, A. A. Guda, V. Shapovalov, R. Witter, M. Fichtner, H. Hahn, *Phys. Chem. Chem. Phys.* **2015**, 17, 17288.

- [8] N. Yabuuchi, M. Takeuchi, M. Nakayama, H. Shiiba, M. Ogawa, K. Nakayama, T. Ohta, D. Endo, T. Ozaki, T. Inamasu, K. Sato, S. Komaba, *Proc. Natl. Acad. Sci. USA* **2015**, *112*, 7650.
- [9] R. Wang, X. Li, L. Liu, J. Lee, D.-H. Seo, S.-H. Bo, A. Urban, G. Ceder, *Electrochem. Commun.* **2015**, *60*, 70.
- [10] S. L. Glazier, J. Li, J. Zhou, T. Bond, J. R. Dahn, *Chem. Mater.* **2015**, *27*, 7751.
- [11] J. Lee, D.-H. Seo, M. Balasubramanian, N. Twu, X. Li, G. Ceder, *Energy Environ. Sci.* **2015**, *8*, 3255.
- [12] V. Pralong, V. Gopal, V. Caignaert, V. Duffort, B. Raveau, *Chem. Mater.* **2012**, *24*, 12.
- [13] K. Mizushima, P. Jones, P. Wiseman, J. Goodenough, *Mater. Res. Bull.* **1980**, *15*, 783.
- [14] M. Thackeray, W. David, P. Bruce, J. Goodenough, *Mater. Res. Bull.* **1983**, *18*, 461.
- [15] A. Urban, J. Lee, G. Ceder, *Adv. Energy Mater.* **2014**, *4*, 1400478.
- [16] M. M. Thackeray, S.-H. Kang, C. S. Johnson, J. T. Vaughney, R. Benedek, S. A. Hackney, *J. Mater. Chem.* **2007**, *17*, 3112.
- [17] J. Hong, H. Gwon, S.-K. Jung, K. Ku, K. Kang, *J. Electrochem. Soc.* **2015**, *162*, A2447.
- [18] P. Rozier, J. M. Tarascon, *J. Electrochem. Soc.* **2015**, *162*, A2490.
- [19] N. Tran, L. Croguennec, M. Ménétrier, F. Weill, P. Biensan, C. Jordy, C. Delmas, *Chem. Mater.* **2008**, *20*, 4815.
- [20] B. Xu, C. R. Fell, M. Chi, Y. S. Meng, *Energy Environ. Sci.* **2011**, *4*, 2223.
- [21] M. Sathiyaraj, A. M. Abakumov, D. Foix, G. Rousse, K. Ramesha, M. Saubanère, M. Doublet, H. Vezin, C. P. Laisa, A. S. Prakash, D. Gonbeau, G. VanTendeloo, J.-M. Tarascon, *Nat. Mater.* **2014**, *14*, 230.
- [22] J. Zheng, P. Xu, M. Gu, J. Xiao, N. D. Browning, P. Yan, C. Wang, J.-G. Zhang, *Chem. Mater.* **2015**, *27*, 1381.
- [23] J. C. Bachman, S. Muy, A. Grimaud, H.-H. Chang, N. Pour, S. F. Lux, O. Paschos, F. Maglia, S. Lupart, P. Lamp, L. Giordano, Y. Shao-Horn, *Chem. Rev.* **2016**, *116*, 140.
- [24] J. Li, C. Ma, M. Chi, C. Liang, N. J. Dudney, *Adv. Energy Mater.* **2015**, *5*, 1401408.
- [25] J. Reed, G. Ceder, *Chem. Rev.* **2004**, *104*, 4513.
- [26] J. Reed, G. Ceder, *Electrochem. Solid-State Lett.* **2002**, *5*, A145.
- [27] S. Prabaharan, M. Michael, H. Ikuta, Y. Uchimoto, M. Wakihara, *Solid State Ionics* **2004**, *172*, 39.
- [28] L. Zhang, H. Noguchi, D. Li, T. Muta, X. Wang, M. Yoshio, I. Taniguchi, *J. Power Sources* **2008**, *185*, 534.
- [29] M. Tabuchi, A. Nakashima, H. Shigemura, K. Ado, H. Kobayashi, H. Sakaebe, K. Tatsumi, H. Kageyama, T. Nakamura, R. Kanno, *J. Mater. Chem.* **2003**, *13*, 1747.
- [30] H. Shigemura, M. Tabuchi, H. Sakaebe, H. Kobayashi, H. Kageyama, *J. Electrochem. Soc.* **2003**, *150*, A638.
- [31] M. Obrovac, O. Mao, J. Dahn, *Solid State Ionics* **1998**, *112*, 9.
- [32] P. Hohenberg, W. Kohn, *Phys. Rev.* **1964**, *136*, B864.
- [33] W. Kohn, L. J. Sham, *Phys. Rev.* **1965**, *140*, A1133.
- [34] J. Perdew, K. Burke, M. Ernzerhof, *Phys. Rev. Lett.* **1996**, *77*, 3865.
- [35] J. Perdew, K. Burke, M. Ernzerhof, *Phys. Rev. Lett.* **1997**, *78*, 1396.
- [36] P. E. Blöchl, *Phys. Rev. B* **1994**, *50*, 17953.
- [37] G. Kresse, J. Furthmüller, *Comput. Mater. Sci.* **1996**, *6*, 15.
- [38] G. Kresse, J. Furthmüller, *Phys. Rev. B* **1996**, *54*, 11169.
- [39] M. Cococcioni, S. de Gironcoli, *Phys. Rev. B* **2005**, *71*, 035105.
- [40] V. I. Anisimov, F. Aryasetiawan, A. I. Lichtenstein, *J. Phys.: Condens. Matter* **1997**, *9*, 767.
- [41] A. Jain, G. Hautier, C. J. Moore, S. P. Ong, C. C. Fischer, T. Mueller, K. A. Persson, G. Ceder, *Comput. Mater. Sci.* **2011**, *50*, 2295.
- [42] S. P. Ong, W. D. Richards, A. Jain, G. Hautier, M. Kocher, S. Cholia, D. Gunter, V. L. Chevrier, K. A. Persson, G. Ceder, *Comput. Mater. Sci.* **2013**, *68*, 314.
- [43] J. Sanchez, F. Ducastelle, D. Gratias, *Phys. A* **1984**, *128*, 334.
- [44] D. D. Fontaine, *Solid State Phys.* **1994**, *47*, 33.
- [45] W. Li, J. N. Reimers, J. R. Dahn, *Phys. Rev. B* **1994**, *49*, 826.
- [46] CASM, v0.1.0, <https://github.com/prisms-center/CASMcode> (accessed: September 2015).
- [47] B. Puchala, A. Van der Ven, *Phys. Rev. B* **2013**, *88*, 094108.
- [48] J. C. Thomas, A. Van der Ven, *Phys. Rev. B* **2013**, *88*, 214111.
- [49] A. Van der Ven, J. Thomas, Q. Xu, J. Bhattacharya, *Math. Comput. Simul.* **2010**, *80*, 1393.
- [50] G. L. W. Hart, R. W. Forcade, *Phys. Rev. B* **2008**, *77*, 224115.
- [51] G. L. W. Hart, R. W. Forcade, *Phys. Rev. B* **2009**, *80*, 014120.
- [52] G. L. Hart, L. J. Nelson, R. W. Forcade, *Comput. Mater. Sci.* **2012**, *59*, 101.
- [53] L. J. Nelson, G. L. W. Hart, F. Zhou, V. Ozolinš, *Phys. Rev. B* **2013**, *87*, 035125.
- [54] A. Zunger, S.-H. Wei, L. G. Ferreira, J. E. Bernard, *Phys. Rev. Lett.* **1990**, *65*, 353.
- [55] D. Shin, A. van de Walle, Y. Wang, Z.-K. Liu, *Phys. Rev. B* **2007**, *76*, 144204.
- [56] S.-H. Wei, L. G. Ferreira, J. E. Bernard, A. Zunger, *Phys. Rev. B* **1990**, *42*, 9622.
- [57] C. Wolverton, *Acta Mater.* **2001**, *49*, 3129.
- [58] A. van de Walle, P. Tiwary, M. de Jong, D. Olmsted, M. Asta, A. Dick, D. Shin, Y. Wang, L.-Q. Chen, Z.-K. Liu, *Calphad* **2013**, *42*, 13.
- [59] T. Hewston, B. Chamberland, *J. Phys. Chem. Solids* **1987**, *48*, 97.
- [60] A. Van der Ven, G. Ceder, *Electrochem. Commun.* **2004**, *6*, 1045.
- [61] G. Hautier, S. P. Ong, A. Jain, C. J. Moore, G. Ceder, *Phys. Rev. B* **2012**, *85*, 155208.
- [62] H. Wang, Y. Jang, B. Huang, D. R. Sadoway, Y. Chiang, *J. Electrochem. Soc.* **1999**, *146*, 473.
- [63] C. Delmas, J. P. Pérès, A. Rougier, A. Demourgues, F. Weill, A. Chadwick, M. Broussely, F. Perton, P. Biensan, P. Willmann, *J. Power Sources* **1997**, *68*, 120.
- [64] M. Yang, X. Zhao, Y. Bian, L. Ma, Y. Ding, X. Shen, *J. Mater. Chem.* **2012**, *22*, 6200.
- [65] D. R. Modeshia, R. I. Walton, M. R. Mitchell, S. E. Ashbrook, *Dalton Trans.* **2010**, *39*, 6031.
- [66] J. Anderson, M. Schieber, *J. Phys. Chem. Solids* **1964**, *25*, 961.
- [67] H. J. T. Ellingham, *J. Soc. Chem. Ind.* **1944**, *63*, 125.
- [68] R. D. Shannon, *Acta Crystallogr., Sect. A* **1976**, *32*, 751.
- [69] Materials Project, <http://www.materialsproject.org> (accessed: February 2016).
- [70] A. Jain, S. P. Ong, G. Hautier, W. Chen, W. D. Richards, S. Dacek, S. Cholia, D. Gunter, D. Skinner, G. Ceder, K. A. Persson, *APL Mater.* **2013**, *1*, 011002.
- [71] S. P. Ong, L. Wang, B. Kang, G. Ceder, *Chem. Mater.* **2008**, *20*, 1798.
- [72] FIZ Karlsruhe, <http://icsd.fiz-karlsruhe.de> (accessed: February 2016).
- [73] G. Bergerhoff, R. Hundt, R. Sievers, I. Brown, *J. Chem. Inf. Comput. Sci.* **1983**, *23*, 66.
- [74] J. Cho, Y. J. Kim, T.-J. Kim, B. Park, *Angew. Chem., Int. Ed.* **2001**, *40*, 3367.